Theor Chem Acc (2012) 131:1204
DOI 10.1007/s00214-012-1204-0

REGULAR ARTICLE

New insights into the mechanism of the Schiff base formation catalyzed by type I dehydroquinate dehydratase from *S. enterica*

Qi Pan · Yuan Yao · Ze-Sheng Li

Received: 13 January 2012 / Accepted: 8 March 2012 / Published online: 27 March 2012

Abstract The Schiff base formation catalyzed by type I dehydroquinate dehydratase (DHQD) from *Salmonella enterica* has been studied by molecular docking, molecular dynamics simulation, and quantum chemical calculations. The substrate locates stably a similar position as the Schiff base intermediate observed in the crystal structure and forms strong hydrogen bonds with several active site residues. This binding mode is different from that of several other Schiff base enzymes. Then, the quantum chemical model has been constructed and the fundamental reaction pathways have been explored by performing quantum chemical calculation. The energy barrier of the previously proposed reaction pathway is calculated to be 30.7 kcal/mol, which is much higher than the experimental value of 14.3 kcal/mol of the whole dehydration reaction by type I DHQD from *S. enterica*. It means that this pathway is not favorable in energy. Therefore, a new and unexpected reaction pathway has been investigated with the favorable and reasonable energy barrier of 12.1 kcal/mol. The complicated role of catalytic His143 residue has also been elucidated that it mediates two proton transfers to facilitate the reaction. Moreover, the similarity and the difference between these two reaction pathways have been analyzed in detail. The new structural and mechanistic insights may direct the design of the inhibitors of type I dehydroquinate dehydratase as non-toxic antimicrobials, antifungals, and herbicides.

Keywords Dehydroquinate dehydratase · Binding mode · Enzymatic reaction mechanism · Molecular docking · Molecular dynamics simulation · Quantum chemical calculation

Q. Pan · Y. Yao (✉) · Z.-S. Li
Academy of Fundamental and Interdisciplinary Science, Harbin Institute of Technology, Harbin 150080, People's Republic of China
e-mail: yyuan@hit.edu.cn

Q. Pan
Department of Orthopaedic, The First Affiliated Hospital of Harbin Medical University, Harbin 150080, People's Republic of China

Z.-S. Li (✉)
Key Laboratory of Cluster Science of Ministry of Education, School of Chemistry, Beijing Institute of Technology, No. 5 Yard, Zhong Guan Cun South Street, Beijing 100081, People's Republic of China
e-mail: zeshengli@bit.edu.cn

1 Introduction

The biosynthetic shikimate pathway is present in bacteria, fungi, and plants but absent in mammals. Its end product, chorismate, is a critical precursor of many biologically important aromatic compounds such as aromatic amino acid, ubiquinones, vitamin E, and folates [1]. So the enzymes involved in this pathway are considered as the potential targets for the design of the high-activity inhibitors as non-toxic antimicrobials, antifungals, and herbicides [2, 3].

The third step in the shikimate pathway, the dehydration of dehydroquinate to dehydroshikimate, is catalyzed by dehydroquinate dehydratase (DHQD; EC 4.2.1.10). So far, two distinct types of DHQDs (termed type I and type II) have been identified to catalyze the same dehydration reaction, but they neither share any sequence similarities nor employ the same mechanism [4–7]. Type I DHQD undergoes a cis-elimination through a covalent Schiff base intermediate formed between the highly conserved Lys170

residue and the substrate. The entire reaction consists of three processes, the Schiff base formation, the dehydration, and the Schiff base hydrolysis. In contrast, type II DHQD undergoes a trans-elimination without the covalent Schiff base intermediate. Therefore, it is of great mechanistic and evolutionary interest to explore the structure and mechanism of DHQDs to understand how this situation arises and further design new inhibitors. The results of several chemical modification and mutagenesis experiments clearly suggest that the Schiff base intermediate not only simply holds the substrate in the active site, but also plays important catalytic roles in the dehydration process [8, 9]. This suggestion is also supported by the observed conformations in the recently reported crystal structures of type I DHQD from *Salmonella enterica* (PDB code: 3M7W and 3NNT) that the substrate adopts the similar position both in the Schiff base intermediate and in K170 M mutant with non-covalent complex [10]. However, the reaction mechanism of the Schiff base formation is not very clear so far. First, how does the Schiff base formation occurs? According to the stereoelectronic principles, it is possible for the highly conserved Lys170 residue to approach the *3*-carbonyl carbon (C_3) atom of the substrate at the Bürgi–Dunitz angle of $\sim 107°$ [11] and form the covalent Schiff base between them. However, modeling Lys170 to the crystal structure of K170 M mutant in non-covalent complex shows that the maximal approach angle of the NZ atom in Lys170, the C_3 atom in the substrate, and the *3*-carbonyl oxygen (O_3) atom in the substrate (NZ–C_3–O_3) is 58° [10], which is much less than the Bürgi–Dunitz angle. Thus, the covalent Schiff base may form either by a non-Bürgi–Dunitz approach with the substrate in its observed position or by a Bürgi–Dunitz approach with the substrate in its unobserved position in the active site. In the latter case, during the process of the substrate docking into the active site, the substrate reaches a first binding position where the Bürgi–Dunitz angle requirement is met and the covalent Schiff base is formed and then reorganizes its position to be the observed one in the crystal structure of type I DHQD from *S. enterica* with the Schiff base intermediate [10]. In fact, this suggested binding mode is found in the Schiff base formation catalyzed by several other enzymes, such as fructose 1,6-bisphosphate aldolase [12], dihydrodipicolinate synthase [13], and 2-keto-3-deoxy-6-phosphogluconate aldolase [14]. The crystallographic studies of these enzymes indicate that the orientation of the substrate in Schiff base intermediate is rotated $\sim 180°$ in the active site by comparing with the non-bound substrate. It is not clear whether this mode is general to all enzymes that catalyze the Schiff base formation or not. Second, the catalytic role of His143 is not clear. On the basis of site-directed mutagenesis, Leech et al. [9] proposed a reaction pathway (shown in Scheme 1) in which His143 acts as a general acid to facilitate the protonation of the carbinolamine intermediate in the second step. The crystal structure of K170 M mutant of type I DHQD from *S. enterica* in non-covalent complex with dehydroquinate indicates that the position of His143 is proximal to the O_3 atom. This conformation implies that His143 not only protonates the O_3 atom but also enhances the dipole of the carbonyl group by drawing away from the C_3 atom, which may facilitate the nucleophilic attack on the C_3 atom by Lys170. It further suggests that His143 may play more catalytic roles in the Schiff base formation than that in Scheme 1.

The focus of the present study is the mechanism of the Schiff base formation by type I DHQD. The multiscale computational methods, such as molecular docking, molecular dynamics simulation, and quantum chemical calculation, were used to explore the binding mode and the detailed mechanism of the Schiff base formation by type I DHQD on the basis of the crystal structure of K170 M mutant of type I DHQD from *S. enterica* in non-covalent complex with dehydroquinate (PDB code: 3NNT).

1.1 Computational details

1.1.1 Structure preparation

The initial structure of the substrate is from the crystal structure of K170 M mutant of type I DHQD from *S. enterica* with non-covalent complex with dehydroquinate (PDB code: 3NNT) [10], and the initial structure of the wild type enzyme is generated on the basis of the same crystal structure through replacing Met170 by Lysine. The ionization states of His143 and Lys170 were set on the basis of the experimental studies [9, 15–17]. The ionization states of other ionizable residues were determined on the basis of the pK_a value estimated by PROPKA program [18–21].

1.1.2 Molecular docking

In order to explore the binding mode of type I DHQD with the substrate dehydroquinate, the docking program AUTODOCK 4.2 [22] with the genetic algorithm method was used to perform the automated molecular docking. The polar hydrogen atoms of the enzyme were added. The grid box dimensions were $60 \times 60 \times 60$ Å around the active site, and the grid spacing was 0.375 Å. The standard docking protocol for flexible ligand docking consisted of 50 independent runs, using an initial population of 150 randomly placed individuals, with 2,500,000 energy evaluations, a max number of 27,000 iterations, a mutation rate of 0.02, a crossover rate of 0.8. After docking, RMS deviation with the value of 1 Å was used

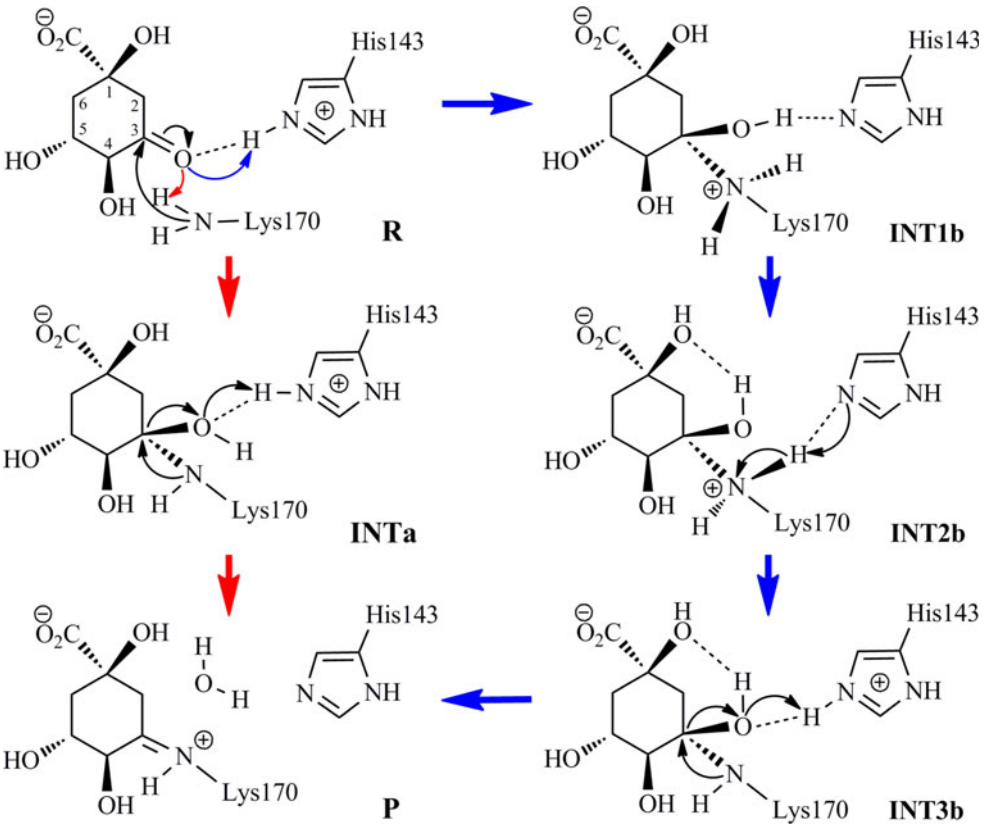

Scheme 1 The reaction mechanisms of Schiff base formation by type I DHQD. The previously proposed reaction pathway is labeled by the *red arrows*, and the new one is labeled by the *blue arrows*

for the cluster analysis with the reference to the starting conformation. Finally, the conformation with the lowest binding energy in each cluster was considered as the most trustable solution.

1.1.3 Molecular dynamics simulation

The docking confirmation was selected as the initial structure of the MD simulation. All missing hydrogen atoms were added by LEaP module in Amber 9 package [23, 24]. The system was then solvated in a rectangular box of TIP3P water molecules [25] with a minimum solute wall distance of 10 Å. The prepared system was fully energy minimized followed by the equilibration through gradually increasing the temperature from 10 to 298.15 K. Then, the production MD simulation was kept running for ~2 ns. During MD simulation, the time step was set as 2 fs with a cutoff of 10 Å for non-bond interactions. The shake procedure [26, 27] was employed to constrain all bonds involving hydrogen atoms. The MD simulation was performed by the Sander module in Amber9 package [23, 24]. The partial atomic charges for the atoms in the substrate were calculated by using the RESP protocol implemented in the Antechamber module in Amber9 package [23, 24] after electrostatic potential (ESP) calculation at B3LYP/6-31G* level using Gaussian 03 program [28].

1.1.4 Quantum chemical calculations

All quantum chemical calculations presented here were performed using the density functional theory B3LYP as implemented in Gaussian 03 program [28]. For geometry optimization, the 6-31G* basis set was used. The initial geometry coordinates were set on the basis of the reaction coordinate involved in the proposed reaction mechanism shown in Scheme 1. Once the geometry optimization was done, the frequency calculation was followed to identify the nature of the stationary point. During the geometry optimizations, the truncated atoms were fixed to prevent unrealistic movements of the various groups in the models. This technology results in a few small imaginary frequencies, which can be ignored because they do not contribute significantly to the energy. In order to obtain more accurate energy, single-point calculations based on the optimized geometries were carried out using B3LYP/6-311+G(2d,2p) level. The solvate effects were calculated at the same level as the geometry optimization by performing single-point calculations on the optimized geometries using the polarizable continuum model method (PCM) [29–31]. Two dielectric constants, 4 and 80, were chosen here to mimic protein environment [32–34] and the water solution, respectively. The dielectric constant of 4 has been widely used to simulate the protein environment because it

typically represents both electronic polarizability and some internal polarization within the protein, as expected for side chain and motions responding to charges. The basis set and the computational method here have been successfully used to study the enzymatic reaction mechanism, and the results are reasonable and reliable [35–39].

2 Results and discussion

2.1 Determination of ionization states

Ionizable residues in proteins, especially in the active sites of enzymes, play important roles for the ligand–enzyme interactions. On the basis of pH/log V_{max} profiles [15] and the pK_a value from diethyl polycarbonate treatment [16], a single ionizing group was measured with a pK_a value of 6.2 and therefore postulated to be His143 residue. However, the pH titration indicated that His143 does not ionize over the pH range of 6–9.5 in the presence and absence of the binding substrate [17], and so cannot possess the pK_a value of 6.2. Thus, the ionization observed with the pK_a value of 6.2 should be associated with a neighboring residue of His143. The crystal structures of type I DHQD (PDB code: 2EGZ and 2YSW) show that the catalytic histidine residue forms a hydrogen bond with the catalytic lysine residue, thus the question arises as to whether this lysine residue could have the pK_a value of 6.2. Normally, the pK_a value of lysine residue is 10.5. If Lys170 has very low pK_a value of 6.2, the enzyme must reduce the normal pK_a value of Lys170 to reach it. It seems very difficult, but it may be achieved by another positively charged Arg82 residue nearby, and this case was also observed in acetoacetate carboxylase [38]. Thus, Lys170 was deprotonated by donating a proton to His143 with the effect of Arg82 residue, resulting in the protonated His143 and deprotonated Lys170. This enables the nucleophilic attack on the carbonyl carbon atom in the substrate by Lys170 residue. Furthermore, the K170A mutant does not affect the isoelectric point of the enzyme [17], meaning that Lys170 residue is likely uncharged. This supports that Lys170 is deprotonated with the low pK_a value of 6.2 and is also in good agreement with the previously proposed mechanism [9]. Therefore, the ionization states of His143 and Lys170 were set to be protonated and deprotonated in the current study, respectively. Furthermore, pH titration clearly indicated that ligand binding does not change the pK_a value of His143 residue [17], which means that His143 residue is also protonated in the absence of the substrate. Thus, it can be concluded that the proton transfer between Lys170 and His143 residues may be driven by ionization equilibration of the solution before the ligand binding, and this process may not affect the free energy of activation for the Schiff base formation.

Table 1 The estimated pK_a values of the ionizable residues in the active site by PROPKA program

	Standard pK_a value	Estimated pK_a value	
		Without substrate	With substrate
His143	6.1	0.9	2.0
Lys170	10.5	7.8	8.5
Glu46	4.5	5.5	4.5
Arg48	12.5	12.1	13.2
Arg82	12.5	13.9	17.2
Arg213	12.5	9.4	9.9

To determine the ionization states of other ionizable residues in the active site of type I DHQD, we employed PROPKA program to estimate the pK_a values of these residues with the initial structure of type I DHQD. As listed in Table 1, the pK_a value of Glu46 was calculated to be 5.5, which is lower than 7.4 of the pH value in the physiological condition. This means that Glu46 is in the deprotonated state. The pKa values of Arg48, Arg82, and Arg213 were calculated to be 12.1, 13.9, and 9.4, respectively, meaning that they are in the protonated state. In addition, the pK_a values of His143 and Lys170 residues were calculated and listed in Table 1, too. It seems that the calculated pK_a values of His143 and Lys170 residues are not consistent with the determined ionization states of His143 and Lys170 residues discussed above. This case is not surprising because Lys170 has an unusual ionization state, further affecting the pK_a value of His143 residue. His143 has a low pK_a value of 2.0, indicating that histidine residue has the uncertainties in the predicted pK_a value by the PROPKA program. The theoretical pK_a estimation usually cannot specialize this kind of case.

2.2 Substrate binding analysis

To address the mechanistic questions related to the Schiff base formation involved in the dehydration reaction catalyzed by type I DHQD, we investigated the possible binding modes of the substrate by performing the molecular docking. The docking result indicates that two completely different clusters (termed ***a*** and ***b***, respectively) of the enzyme–substrate complex, which consists of 35 and 15 independent docking simulation runs, respectively, has been revealed. The conformations which have the lowest binding energies in the each cluster of −8.84 and −7.63 kcal/mol, respectively, are shown in Fig. 1a. In conformation ***a***, the substrate is locating in the similar position as that in the crystal structures of the Schiff base

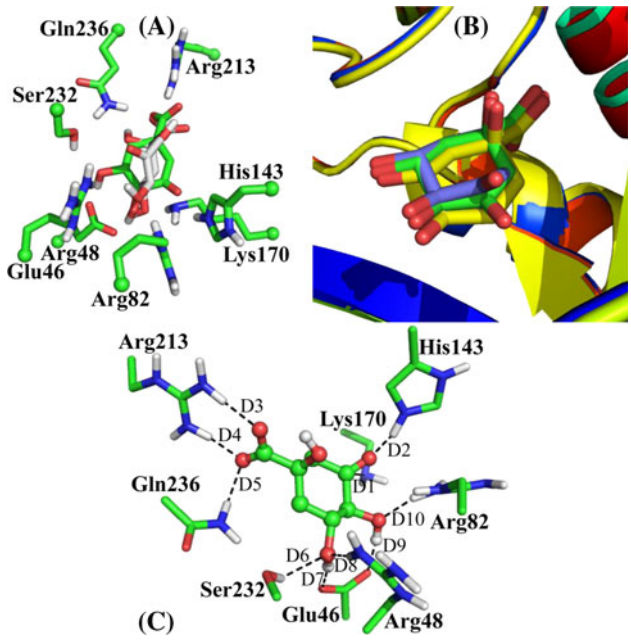

Fig. 1 **a** The docking conformations *a* and *b* of the enzyme–substrate complexes with the carbon atoms in the substrate in *blue* and *white*, respectively. **b** The superimposed conformations of the docking conformation *a*, and the crystal structure of type I DHQD from *S. enterica* in the Schiff base intermediate (PDB code: 3M7W), and the crystal structure of the K170M mutant of type I DHQD from *S. enterica* with non-covalent complex (PDB code: 3NNT). **c** The hydrogen bond interactions between the substrate and the active site residues in conformation *a*

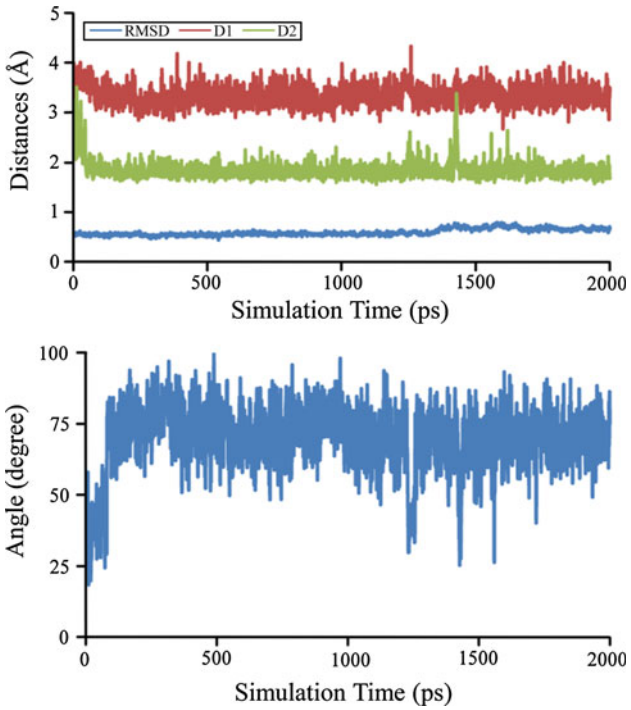

Fig. 2 The key distances during the MD simulation. The distances between the NZ atom in Lys170 and the C_3 atom in the substrate (termed D1), and between the O_3 atom in the substrate and the $H^{\varepsilon 2}$ atom in His143 (termed D2) are listed in the upper. The angle of the NZ atom in Lys170, the C_3 atom, and the O_3 atom in the substrate is listed in the bottom. The distances are in angstrom, and the angle is in degree

intermediate (3M7W) and the K170 M mutant with the non-covalent substrate (3NNT) (As shown in Fig. 1b). The distance between the C_3 and NZ atom is 3.04 Å in conformation *a* (not shown in Fig. 1a). In contrast, for conformation *b*, the orientation of the substrate is rotated $\sim 90^{\circ}$ within the active site when compared with confirmation *a*, and this makes 3-carbonyl group locating away from Lys170. The distance between the C_3 and NZ atom is elongated to be 5.89 Å (not shown in Fig. 1a) in conformation *b*, which is much longer than that in conformation *a*. On the basis of the binding energy and the conformation analysis, it can be reasonably concluded that conformation *b* is not suitable for the formation of Schiff base intermediate and therefore ignored. The enzyme–substrate interaction analysis shows that the substrate forms strong hydrogen bonds with several active site residues as shown in Fig. 1c. These hydrogen bonds play key roles to hold the substrate and stabilize the enzyme–substrate complex. Conclusively, conformation *a* is the only binding mode of the substrate, and there is no any other possible position for the substrate to form the covalent Schiff base with the enzyme. It further means that the formation of the covalent Schiff base occurs until the substrate reaches the corresponding position in the crystal structure. This conclusion cannot support the hypothesis described above that the covalent Schiff base adduct may form before the substrate reaches its observed position in the crystal structure of the Schiff base intermediate (3M7W) [10]. This mode is special to type I DHQD by compared with several enzymes mentioned above that generate a similar Schiff base intermediate.

In order to check whether the states of the ionizable residues in the active site were affected by the binding of the substrate, the pK_a values of these residues in conformation *a* were recalculated by performing PROPKA program. As shown in Table 1, they are close to those without the substrate except Arg82 residue. The pK_a value of Arg82 was increased to be 17.2 by the substrate docking. Through the hydrogen bond interaction with the substrate, the positive charge on Lys170 was stabled and this may decrease the ionization, resulting in a higher pK_a value. Overall, the ionization states of these residues are not qualitatively changed by the substrate. Then, the molecular dynamics simulation was performed on conformation *a* to test the stability. A $\sim$2-ns simulation should be adequate in sampling the orientation of the substrate in the active site. As shown in Fig. 2, the time-dependent RMSD curve to track the Cα atoms in the enzyme did not significantly

Table 2 The average distances of the hydrogen bonds between the substrate and the active sites residues during MD simulation

Labels	Hydrogen bonds	Distance (Å)
D3	Arg213–2HH2···OE2–C–C_1–substrate	1.84 ± 0.11
D4	Arg213–2HH1···OE1–C–C_1–substrate	1.84 ± 0.10
D5	Gln236–2HE2···OE1–C–C_1–substrate	1.92 ± 0.17
D6	Ser232–HG···O–C_5–substrate	2.32 ± 0.40
D7	Glu46–OE1···HO–C_5–substrate	1.73 ± 0.15
D8	Glu46–OE2···HO–C_4–substrate	1.64 ± 0.09
D9	Arg48–1HH1···O–C_5–substrate	1.95 ± 0.13
D10	Arg82–1HH2···O–C_4–substrate	1.93 ± 0.13

change, meaning that the enzyme is very stable and the conformation of the enzyme did not significantly change during the simulation. In order to check the stability of enzyme–substrate complex, the hydrogen bond interactions between the substrate and the active site residues shown in Fig. 1b have been analyzed in detail. As listed in Table 2, the substrate forms very strong hydrogen bonds with the active site residues, and these distances did not significantly change during the simulation. It is evident that the enzyme–substrate complex is very stable and the substrate almost keeps in its docking position. In addition, the average distance between the NZ atom in Lys170 and the C_3 atom in the substrate is ~3.3 Å. A strong hydrogen bond is formed between the O_3 atom in the substrate and the $H^{\varepsilon 2}$ atom in His143 with the average distance of ~1.85 Å. The average angle of NZ–C_3–O_3 is ~75°. Apparently, this does not meet the requirement of Bürgi–Dunitz approach. Then, a snapshot whose conformation is close to the average structure in the simulation was chosen as the initial conformation for the quantum chemical calculations to explore possible reaction mechanism.

2.3 Fundamental reaction mechanism

On the basis of the selected snapshot from molecular dynamics simulation, a quantum chemical model was constructed and it consists of the substrate and the side chains of eight active site residues. On the basis of this model, the fundamental reaction mechanisms have been explored by performing quantum chemical calculations. The results indicate that the previously proposed reaction pathway is unfavorable in energy. Thus, an unexpected and reasonable reaction pathway has been explored. Below we discuss each of them in detail.

2.3.1 The previously proposed reaction pathway

As shown in Scheme 1, the previously proposed reaction pathway consists of two reaction steps. The first step is the nucleophilic attack on the C_3 atom by the deprotonated Lys170 residue with the simultaneous transfer of a proton from the amide group of Lys170 to the O_3 atom in the substrate. The second step is the C_3–O_3 bond cleavage and the simultaneous generation of a water molecule by accepting a proton from the protonated His143 residue. To confirm whether this reaction pathway is feasible in structure and energy, it was tested by performing quantum chemical calculations and the optimized geometries of all stationary points are shown in Fig. 3. In the reactant (**R**), the distance between the NZ atom in Lys170 and the C_3 atom in the substrate is 2.69 Å, and the distance between the O_3 atom in the substrate and the $H^{\varepsilon 2}$ atom in His143 is 1.64 Å. The angle of NZ–C_3–O_3 is 98.0°, which is much bigger than that in the molecular dynamics simulation. While the nucleophilic attack on the C_3 atom by the NZ atom in Lys170, the distance between the NZ atom in Lys170 and the C_3 atom in the substrate is shortened to be 1.49 Å and the angle of NZ–C_3–O_3 is also reduced to be 91.2° in **TS1a**. Then, a NZ–C_3 single bond is formed between Lys170 and the substrate with the bond length of 1.46 Å in **INTa**. A proton in the amide group in Lys170 has been completely transferred to the O_3 atom in the substrate. In addition, the C_3–O_3 double bond in the substrate is weakened to be a single bond with the bond length of 1.43 Å in **INTa**. For the second reaction step, The C_3–O_3 bond in the substrate is gradually elongated while the $H^{\varepsilon 2}$ atom in His143 transfers to the O_3 atom in the substrate. These lead to the break of the C_3–O_3 bond and the generation of a water molecule. In the product (**P**), the NZ–C_3 bond is strengthened to be a double bond with the distance of 1.29 Å, indicating that the Schiff base intermediate is formed. As shown in Fig. 4, the first step is the rate-determining step and the calculated energy barrier is 29.4 kcal/mol in the gas phase. The energy barriers in the protein environment and the water solution were calculated to be 30.7 and 33.7 kcal/mol. However, both of them are much higher than the experimental value of 14.3 kcal/mol estimated from the value of 210 s^{-1} for k_{cat} of the whole dehydration reaction by type I DHQD from *S. enterica* [10]. This means that this pathway is unfavorable in energy and cannot reflect the nature of the Schiff base formation.

2.3.2 A new and unexpected reaction pathway

A new and unexpected reaction pathway has been explored and shown also in Scheme 1. This reaction pathway consists of four reaction steps. The first step is the nucleophilic attack on C_3 atom by Lys170, the second step is the conformational reorganization, the third step is the proton transfer, and the last step is the formation of the Schiff base intermediate. The optimized geometries of the transition states and the intermediates are shown in Fig. 5.

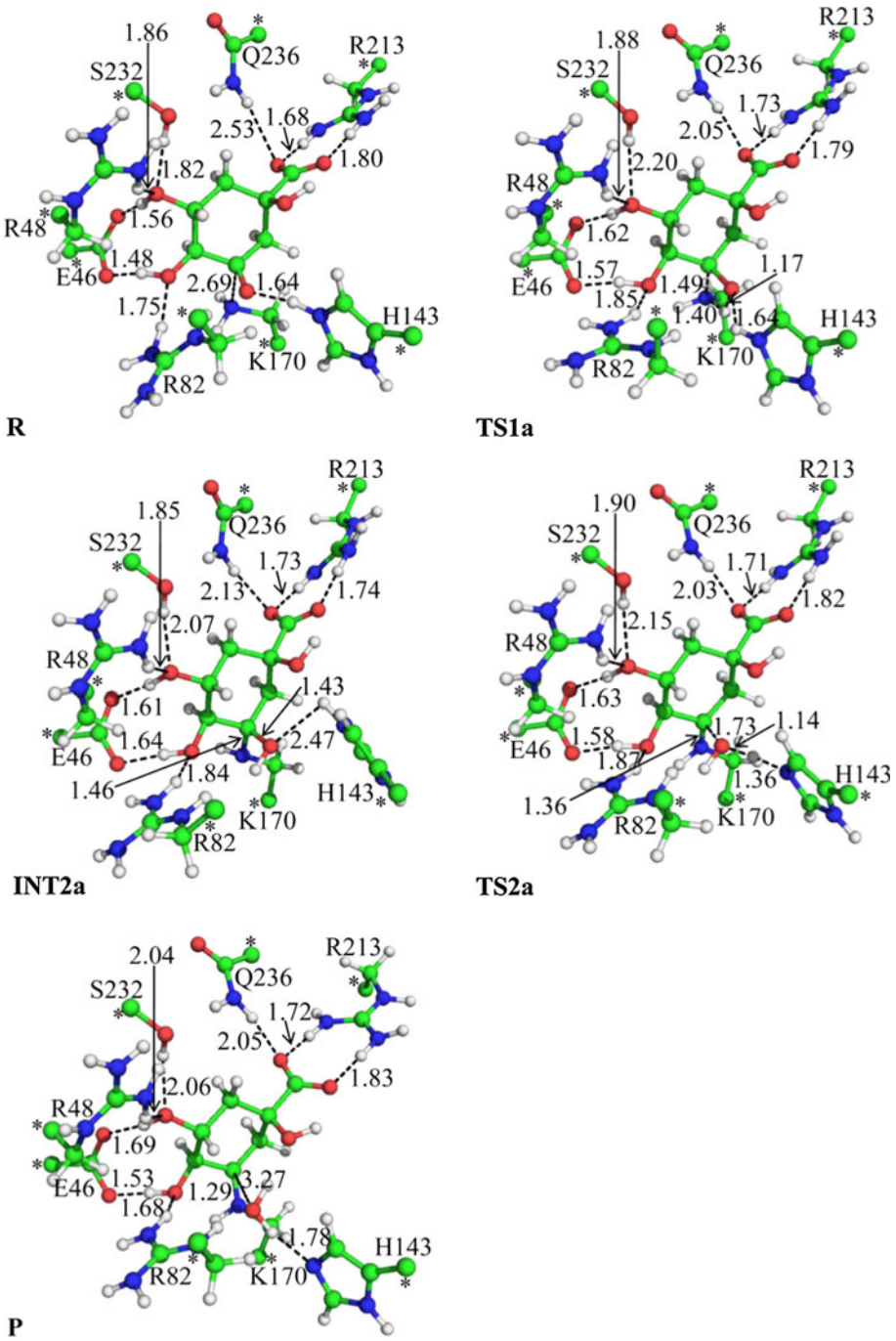

Fig. 3 The optimized geometries involved in the previously proposed reaction mechanism. The distances are in angstrom. Carbon, oxygen, nitrogen, and hydrogen atoms are *colored* in *green*, *red*, *blue*, and *white*, respectively. The carbon atoms labeled by *asterisk* are fixed during the geometry optimization. Figure 5 is represented using the same method

The nucleophilic attack proceeds as the NZ atom in Lys170 gradually approaches the C_3 atom in the substrate. In the mean time, the $H^{\varepsilon 2}$ proton in His143 gradually moves toward the O_3 atom in the substrate. As the nucleophilic attack by NZ atom in Lys170, the C_3 atom is changed to be sp^3-hybridized with a tetrahedral geometry in **INT1b** from a planar geometry centering on the sp^2-hybridized C_3 atom in **R**. In **INT1b**, the length of the NZ–C_3 single bond is 1.56 Å. The $H^{\varepsilon 2}$ proton in His143 has been transferred to the O_3 atom and a single bond forms between them with the bond length of 1.01 Å in **INT1b**. The $H^{\varepsilon 2}$ atom also forms a strong hydrogen bond with the $N^{\varepsilon 2}$ atom in His143 in **INT1b**. Note that the angle of NZ–C_3–O_3 in **TS1b** is 103.2°, which is very close to Bürgi–Dunitz approach of ~107°. This structural feature suggests that the Schiff base formation catalyzed by type I DHQD undergoes the Bürgi–Dunitz approach. In the second step, *3*-hydroxyl group gradually rotates toward the *1*-hydroxyl oxygen atom in the substrate and the position of one proton (HZ) of the amide group in Lys170 is also reorganized to

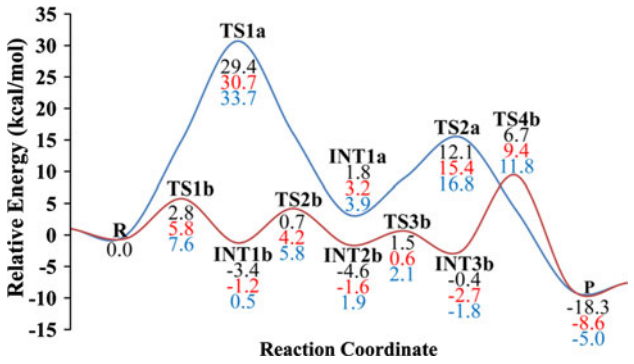

Fig. 4 The calculated potential energy profiles of the previously proposed reaction pathway (*colored* in *blue*) and the new reaction pathway (*colored* in *red*). The energies calculated in the gas phase, in the enzymatic environment, and in the water solution are *colored* in *black*, *red*, and *blue*

be toward the $N^{\varepsilon 2}$ atom in His143. In **INT2b**, *3*-hydroxyl group forms a hydrogen bond with the 1-hydroxyl oxygen atom in the substrate with the distance of 1.76 Å. The HZ atom also forms a strong hydrogen bond with the $N^{\varepsilon 2}$ atom in His143 in **INT2b**, and the hydrogen bond distance is 1.53 Å. This conformation is suitable for the proton transfer involved in the next step. In the third step, the HZ proton is transferred from the NZ atom in Lys170 to the $N^{\varepsilon 2}$ atom in His143, which results in the protonated His143. The C_3–NZ bond is strengthened with the bond length of 1.49 Å in **INT3b**, which is shorter than that in **INT2b**. The HZ atom also forms a strong hydrogen bond with O_3 atom in the substrate with the distance of 2.35 Å. In the last step, the break of C_3–O_3 bond and the $H^{\varepsilon 2}$ proton transfer from His143 to the O_3 atom in the substrate are involved. While the C_3–O_3 bond gradually breaks, the bond of NZ–C_3 is gradually strengthened to be a double bond with the bond length of 1.29 Å, which is shown in Fig. 3. This confirms the formation of the Schiff base intermediate. In the same time, the $H^{\varepsilon 2}$ proton in His143 is simultaneously transferred to the O_3 atom in the substrate, resulting in the generation of a water molecule.

As shown in Fig. 4, in the gas phase, the overall energy barrier for the formation of the Schiff base intermediate by type I DHQD is the energy change from **INT2b** to **TS4b** with the value of 11.3 kcal/mol. However, in the protein environment and the water solution, the overall energy barrier is changed to be the energy change from **INT3b** to **TS4b** of 12.1 and 13.6 kcal/mol, respectively. This result indicates that the solvent effect plays an important role in the third and fourth steps. Notably, the energy barrier in the protein environment of 12.1 kcal/mol is considered as the real energy barrier, and it is lower than the experimental value (14.3 kcal/mol) for the whole dehydration reaction by type I DHQD from *S. enterica* [10] mentioned above. Thus, this new reaction pathway is reasonable and reliable.

It is very interesting to understand the catalytic role of His143. In the new reaction pathway, His143 plays more roles in Schiff base formation than that proposed. In the reactant, His143 is protonated and forms a strong hydrogen bond with the substrate. In the first step, His143 acts as a general acid to donate a proton to the O_3 atom in the substrate when the nucleophilic attack happens. The Mulliken atomic charges on NZ, C_3, O_3 atoms are −0.72, 0.43, and −0.68 in **TS1a**, and −0.73, 0.51, and −0.64 in **TS1b**, respectively, which means that the proton transfer from His143 strengthens the dipole of the carbonyl group. This is also supported by the calculated dipole moments of C_3–O_3 bond in **TS1a** and **TS1b** through NBO method [40–42] with the value of 2.21 and 3.73 Debye, respectively. This change may facilitate the nucleophilic attack of Lys170 on the C_3 atom. Then, the deprotonated His143 accepts a proton from the amide group in Lys170 as a general base in the third step and further transfers this proton to the 3-hydroxyl group as a general acid. Our result about the role of His143 is consistent with the suggestion mentioned above that His143 may play a catalytic role in an earlier step in the Schiff base formation.

2.3.3 *Comparison of two reaction pathways*

Based on the results above, the previously proposed reaction pathway consists of two reaction steps and the first step is the rate-determining one with the unfavorable energy barrier, whereas the new reaction pathway explored here consists of four reaction steps and the fourth step is the rate-determining one with the reasonable energy barrier. The similarities of these two reactions are the nucleophilic attack on the C_3 atom by Lys170 and the protons transfer to the O_3 atom from both Lys170 and His143. But the order and the process of the protons transfer are definitely different in these two reaction pathways. The remarkable difference is the proton transfer in the first step, and this affects significantly the overall energy barriers of these two reaction pathways. By checking carefully the structures of the stationary points in both reaction pathways, this can be explained reasonably. The first reason is the ability to donate a proton of His143 and Lys170. As mentioned above, His143 is protonated and Lys170 is deprotonated in **R**. In the physiological condition with pH value of 7.4, it is evident that the protonated His143 can more easily donate a proton than the deprotonated Lys170. The second reason is the steric hindrance involved in the proton transfer. The angles of the transferred proton, the O_3 atom, and the C_3 atom are 79.6° and 124.9° in **TS1a** and **TS1b**, respectively. It means that the proton of His143 is locating a more suitable position than Lys170 for the proton transfer. In order to finish the proton transfer, the proton in His143 needs to overcome less steric hindrance to reach the O_3 atom than that in Lys170, and this causes a lower energy

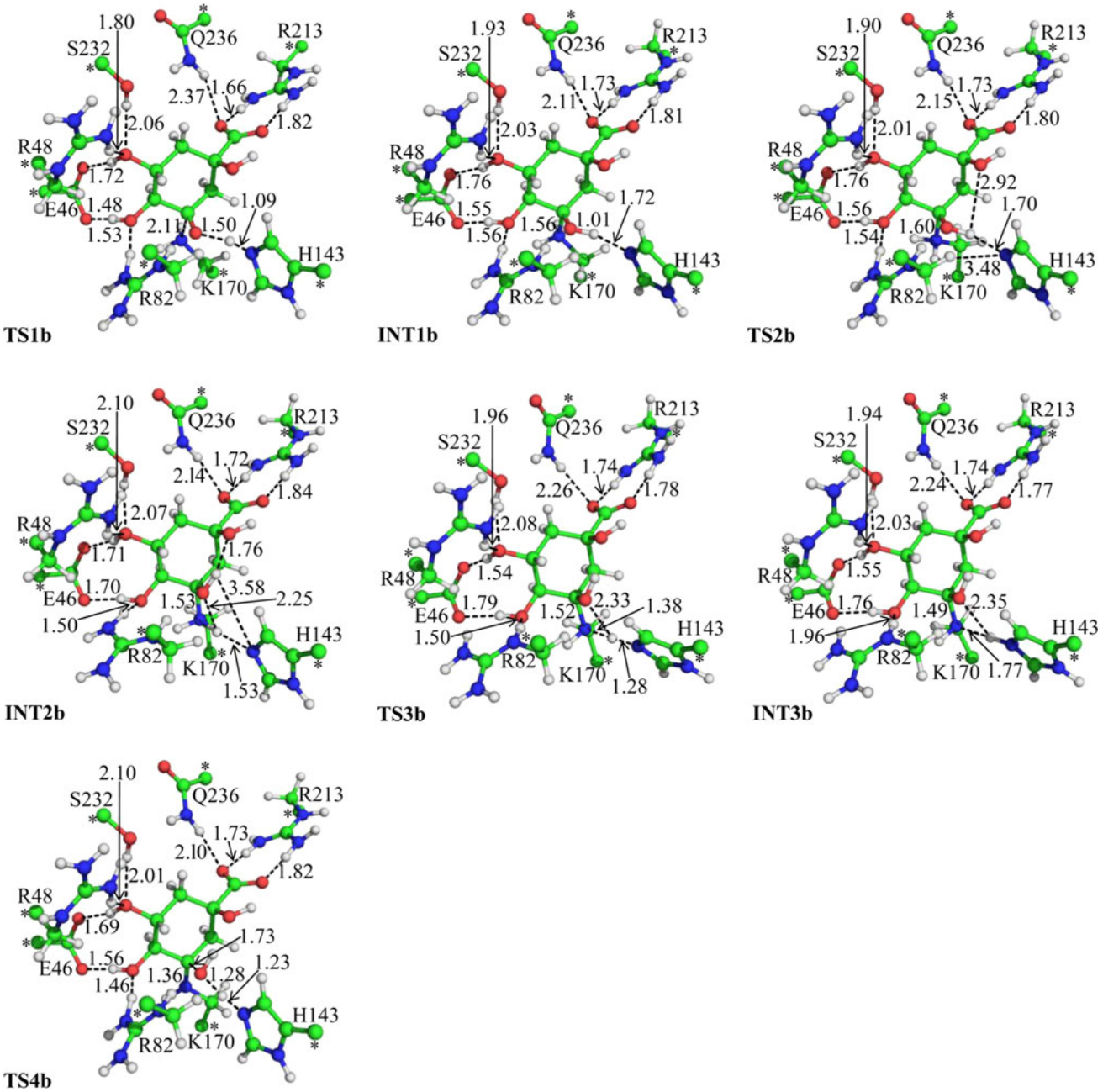

Fig. 5 The optimized geometries of transition states and intermediates involved in the new reaction pathway

barrier. In order to avoid the very high energy barrier caused by the direct proton transfer from Lys170 to the O_3 atom, this process is mediated by His143 in the new reaction pathway. In the first step, the proton transfer between Lys170 and the substrate does not happen. Instead, the protonated His143 donate a proton to the O_3 atom and His143 is in deprotonated state in **INT1b**. The NZ atom in Lys170 possesses a positive charge when forming a single bond with the substrate in **INT1b**, and this strengthens the ability of the NZ atom to donate a proton. After the conformational reorganization and the proton transfer processes with low energy barriers, one proton is transferred to His143 from the NZ atom in Lys170 and His143 is protonated again. This makes the proton locating a suitable position and facilitates the proton transfer to the O_3 atom in the fourth step with a reasonable energy barrier.

3 Conclusion

The multiscale theoretical calculations have been performed to study the reaction mechanism of the Schiff base

formation involved in the dehydration reaction catalyzed by type I DHQD from *S. enterica*. Firstly, the substrate binding analysis using molecular docking and MD simulation indicates that only one binding position of the substrate is suitable for the reaction, and it is very similar to the observed position in the crystal structures of type I DHQD with covalent Schiff base intermediate. This further means that the formation of the Schiff base intermediate cannot occur before the substrate reaches the position observed in the crystal structures. This conclusion negates the previous suggestion which was observed in other Schiff base enzymes that the covalent Schiff base intermediate may form before the substrate reaches its observed position in the crystal structures. Secondly, the fundamental reaction mechanism of Schiff base intermediate formation has been explored by quantum mechanics method. The previously proposed reaction pathway has been tested, and the calculated overall energy barrier is much higher than the experimental value of 14.3 kcal/mol estimated from the value of 210 s^{-1} for k_{cat} of the whole dehydration reaction by type I DHQD from *S. enterica*. This result reveals that this reaction pathway is unfavorable in energy. Thus, a new and unexpected reaction pathway has been explored and elucidated in detail. It consists of four reaction steps. The calculated overall energy barrier of 12.1 kcal/mol is lower than the experimental value of 14.3 kcal/mol of the whole dehydration reaction, meaning that this pathway is reasonable. The catalytic role of His143 has been studied. It mediates two proton transfers and decreases significantly the overall energy barrier. In addition, by comparing with the new reaction pathway, we suggest that the higher energy barrier in the previously proposed reaction pathway is caused by the ability of the proton donor and the steric hindrance in the first step.

The structural and mechanistic insights presented here into the formation of Schiff base by type I DHQD can reasonably explain the known experimental phenomena and may direct the rational design of the new inhibitors of type I DHQD as non-toxic antimicrobials, antifungals, and herbicides.

Acknowledgments This work was supported by the Major State Basic Research Development Programs of China (2011CBA00701), the National Natural Science Foundation of China (20973049), and Development Program for Outstanding Young Teachers in Harbin Institute of Technology (HITQNJS.2009.069).

References

1. Bentley R (1990) Crit Rev Biochem Mol Biol 25:307–384
2. Marques MR, Pereira JH, Oliveira JS, Basso LA, de Azevedo WF, Santos DS, Palma MS (2007) Curr Drug Targets 8(3):445–457
3. Noble M, Sinha Y, Kolupaev A, Demin O, Earnshaw D, Tobin F, West J, Martin JD, Qiu CY, Liu WS, DeWolf WE, Tew D, Goryanin II (2006) Biotechnol Bioeng 95(4):560–573. doi: 10.1002/Bit.20772
4. Butler JR, Alworth WL, Nugent MJ (1974) J Am Chem Soc 96(5):1617–1618
5. Gourley DG, Shrive AK, Polikarpov I, Krell T, Coggins JR, Hawkins AR, Isaacs NW, Sawyer L (1999) Nat Struct Biol 6(6):521–525
6. Kleanthous C, Deka R, Davis K, Kelly SM, Cooper A, Harding SE, Price NC, Hawkins AR, Coggins JR (1992) Biochem J 282:687–695
7. White PJ, Young J, Hunter IS, Nimmo HG, Coggins JR (1990) Biochem J 265(3):735–738
8. Harris J, Kleanthous C, Coggins JR, Hawkins AR, Abell C (1993) Chem Commun 13:1080–1081
9. Leech AP, James R, Coggins JR, Kleanthous C (1995) J Biol Chem 270(43):25827–25836
10. Light SH, Minasov G, Shuvalova L, Duban ME, Caffrey M, Anderson WF, Lavie A (2011) J Biol Chem 286(5):3531–3539
11. Burgi HB, Dunitz JD, Lehn JM, Wipff G (1974) Tetrahedron 30(12):1563–1572
12. Blom N, Sygusch J (1997) Nat Struct Biol 4(1):36–39
13. Soares da Costa TP, Muscroft-Taylor AC, Dobson RCJ, Devenish SRA, Jameson GB, Gerrard JA (2010) Biochimie 92(7):837–845
14. Pohl E, Pauluhn A, Ahmed H, Lorentzen E, Buchinger S, Schomburg D, Siebers B (2008) Proteins 72(1):35–43
15. Chaudhuri S, Lambert JM, Mccoll LA, Coggins JR (1986) Biochem J 239(3):699–704
16. Deka RK, Kleanthous C, Coggins JR (1992) J Biol Chem 267(31):22237–22242
17. Leech AP, Boetzel R, McDonald C, Shrive AK, Moore GR, Coggins JR, Sawyer L, Kleanthous C (1998) J Biol Chem 273(16):9602–9607
18. Li H, Robertson AD, Jensen JH (2005) Proteins 61(4):704–721
19. Bas DC, Rogers DM, Jensen JH (2008) Proteins 73(3):765–783
20. Olsson MHM, Søndergaard CR, Rostkowski M, Jensen JH (2011) J Chem Theory Comput 7(2):525–537
21. Søndergaard CR, Olsson MHM, Rostkowski M, Jensen JH (2011) J Chem Theory Comput 7(7):2284–2295
22. Morris GM, Huey R, Lindstrom W, Sanner MF, Belew RK, Goodsell DS, Olson AJ (2009) J Comput Chem 30(16):2785–2791
23. Case DA, Cheatham TE, Darden T, Gohlke H, Luo R, Merz KM, Onufriev A, Simmerling C, Wang B, Woods RJ (2005) J Comput Chem 26(16):1668–1688
24. Case Dad TA, Cheatham TE, Simmerling CL, Wang J, Duke RE, Luo R, Merz KM, Pearlman DA, Crowley M, Walker RC, Zhang W, Wang B, Hayik S, Roitberg A, Seabra G, Wong KF, Paesani F, Wu X, Brozell S, Tsui V, Gohlke H, Yang L, Tan C, Mongan J, Hornak V, Cui G, Beroza P, Mathews DH, Schafmeister C, Ross WS, Kollman PA (2006) Amber 9. University of California, San Francisco
25. Jorgensen WL, Chandrasekhar J, Madura JD, Impey RW, Klein ML (1983) J Chem Phys 79(2):926–935
26. Miyamoto S, Kollman PA (1992) J Comput Chem 13(8):952–962
27. Ryckaert JP, Ciccotti G, Berendsen HJC (1977) J Comput Phys 23(3):327–341
28. Frisch MJT, G. W, Schlegel HB, Scuseria GE, Robb MA, Cheeseman JR, Montgomery JJA, Vreven T, Kudin KN, Burant JC, Millam JM, Iyengar SS, Tomasi J, Barone V, Mennucci B, Cossi M, Scalmani G, Rega N, Petersson GA, Nakatsuji H, Hada M, Ehara M, Toyota K, Fukuda R, Hasegawa J, Ishida M, Nakajima T, Honda Y, Kitao O, Nakai H, Klene M, Li X, Knox JE, Hratchian HP, Cross JB, Bakken V, Adamo C, Jaramillo J, Gomperts R, Stratmann RE, Yazyev O, Austin AJ, Cammi R, Pomelli C, Ochterski JW, Ayala PY, Morokuma K, Voth GA, Salvador P, Dannenberg JJ, Zakrzewski VG, Dapprich S, Daniels AD, Strain MC, Farkas O, Malick DK, Rabuck AD, Raghavachari K, Foresman JB, Ortiz JV, Cui Q, Baboul AG, Clifford S,

Cioslowski J, Stefanov BB, Liu G, Liashenko A, Piskorz P, Komaromi I, Martin RL, Fox DJ, Keith T, Al-Laham MA, Peng CY, Nanayakkara A, Challacombe M, Gill PMW, Johnson B, Chen W, Wong MW, Gonzalez C, Pople JA (2004) Gaussian 03, Revision E01. Gaussian, Inc., Wallingford CT
29. Cossi M, Barone V, Cammi R, Tomasi J (1996) Chem Phys Lett 255(4–6):327–335
30. Miertus S, Scrocco E, Tomasi J (1981) Chem Phys 55(1):117–129
31. Miertus S, Tomasi J (1982) Chem Phys 65(2):239–245
32. Noodleman L, Lovell T, Han WG, Li J, Himo F (2004) Chem Rev 104(2):459–508
33. Cui FC, Pan XL, Liu W, Liu JY (2011) J Comput Chem 32:3068–3074
34. Himo F, Eriksson LA, Maseras F, Seigbahn PEM (2000) J Am Chem Soc 122:8031–8036
35. Cui FC, Pan XL, Liu JY (2010) J Phys Chem B 114(29):9622–9628
36. Himo F, Chen SL, Marino T, Fang WH, Russo N (2008) J Phys Chem B 112(8):2494–2500
37. Himo F, Liao RZ, Yu JG (2010) Proc Natl Acad Sci USA 107(52):22523–22527
38. Himo F, Liao RZ, Yu JG (2010) J Phys Chem B 114(7):2533–2540
39. Liao RZ, Yu JG, Himo F (2011) J Chem Theory Comput 7(5):1494–1501
40. Highbarger LA, Gerlt JA, Kenyon GL (1996) Biochemistry 35(1):41–46
41. Reed AE, Weinhold F (1985) J Chem Phys 83(4):1736–1740
42. Reed AE, Weinstock RB, Weinhold F (1985) J Chem Phys 83(2):735–746